Nonlinear Dynamics of a Flow-Focusing Bubble Generator: An Inverted Dripping Faucet

Piotr Garstecki,* Michael J. Fuerstman, and George M. Whitesides[†]

Department of Chemistry and Chemical Biology, Harvard University, 12 Oxford Street, Cambridge, Massachusetts 02138, USA
(Received 4 December 2004; published 15 June 2005)

We describe the rich dynamic behavior—including period-doubling and period-halving bifurcations, intermittency, and chaos—observed in the breakup of an inviscid fluid in a coflowing, viscous liquid, both confined in a microfabricated flow-focusing geometry. Experimental observations support inertia-dominated dynamics of the interface, and suggest the possible similarity to the dynamics of a topologically inverted counterpart of this system, that is, a dripping faucet.

This Letter describes rich nonlinear dynamics of bubbling in a microfluidic flow-focusing (FF) device [1–4]. We observe period doubling and halving bifurcations and chaotic bubbling—characteristic features of a model nonlinear system [5–7]. The interesting finding is that, in contrast to earlier work [8], our experimental observations indicate a dynamic similarity to a system that forms the topologically inverted version of our bubble generator—a dripping faucet. In our system gas bubbles into a stream of flowing liquid; in the faucet, liquid drips into ambient gas.

The formation of droplets and bubbles is important to fluid dynamics in two classes of problems: the first deals with interfacial instabilities, and details the asymptotics of pinch off [9–12] of a single drop; the second tries to understand the mechanisms behind the generation of sequences of drops or bubbles [5,13,14]. Systems as simple as a leaky faucet [5,13–18], or a pressurized nozzle releasing gas into a tank of fluid [6,8,19–22] provide archetypal examples of nonlinear dynamics. The behavior of these systems changes dramatically as a control parameter (typically the rate of flow of the fluid that is dispersed) increases above a critical value, and one observes that a series of identical droplets (or bubbles) is replaced by repeating sequences of two, four, or, in general, a number of fluid segments of different sizes. The bifurcations often lead to chaotic behavior characterized by sequences of drops or bubbles with seemingly random sizes. The studies of these phenomena have both fundamental [23,24] and practical [25] implications.

Helsby and Tuson were the first to observe higher-order periodic and chaotic bubbling from a submerged nozzle [6,26]; their observations were followed by more detailed studies by Tritton and Egdell [19], and others [20,27], and the subject is still of significant interest [21,22]. Reports on bubbling from a nozzle describe period-2, period-3, and period-4 attractors, and transitions to chaos—a behavior similar to that of a dripping faucet [5,13,14,16–18]. The study by Nguyen *et al.* [8] suggests, however, that the cause of the instability in a system in which a nozzle injects a train of bubbles into an ambient fluid (a system we refer to as a "vertical nozzle") is different from the cause of bifurcations in the dripping faucet. In the vertical nozzle, instability arises from the movement of bubbles to the top of the fluid; in the faucet system the bifurcations are caused by the dynamics of the oscillating tip [13,14]. As the dynamics of a dripping faucet are well understood [5,13,14,24], it is interesting to ask whether the inverted system (i.e., bubble generator) shares the underlying interplay of forces and relaxation processes that leads to the observed, nonlinear behavior.

The formation of bubbles and droplets in microsystems [1,3,4,28–30] has applications in on-chip separation [31], high-throughput screening [32], protein crystallization [33], kinetic analysis [34], and materials synthesis [35]. A general question in these systems concerns the extent to which the formation of drops can be *controlled,* as breakup is, inherently, a nonlinear phenomenon. Understanding the governing dynamics can help answer whether the nonlinearities can be tamed to yield ideally uniform fluid elements or whether they always introduce higher-order behavior or chaotic responses. A practical goal is to understand the range of parameters (such as the rates of flow, pressures, and viscosities, but also geometry of the device) that promote formation of monodisperse dispersions.

Figure 1(a) shows the FF device [4] that we used. We delivered the fluids to the orifice via three inlet channels—two flanking channels for the continuous fluid, and one central channel for the gas. We used nitrogen and aqueous solutions of glycerol: 0, 30, 58, 62, and 80% (w/w) of viscosities 0.9, 2.5, 5.8, 10.8, 20, and 50 mPa s at 24 °C, respectively [36]. We added 2% (w/w) Tween 20 surfactant to all the solutions to stabilize the bubbles. Gas and liquid form an interface at the junction of the three inlets, upstream of the orifice. Provided that the pressure (p) applied to the gas stream [37] exceeds the pressure required to force the continuous fluid through the outlet channel at the imposed rate of flow (Q), the gaseous thread advances through the orifice into the outlet channel, breaks, releases a bubble, and retracts upstream. The process then repeats.

For a given, fixed value of p, as we gradually increase Q, the system first produces monodisperse bubbles. As Q is raised above a critical value $Q_{CR}(p)$, the breakup process bifurcates and the system produces sequences of two bubbles of different sizes [38]: the thread advances into the
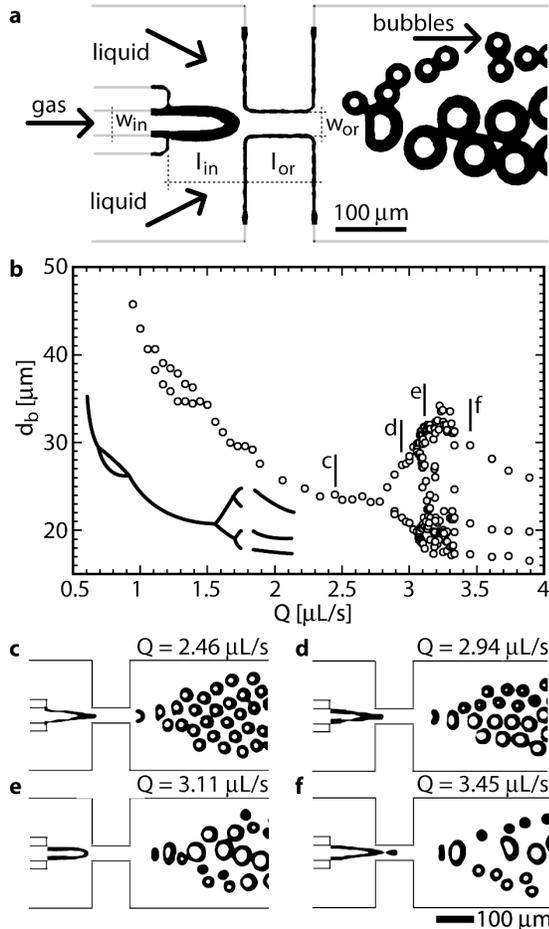
FIG. 1.   (a) An optical micrograph of the FF bubble generator comprising a planar network of channels fabricated in poly(-dimethylsiloxane) and having a uniform height of 25 μm. The relevant dimensions are plotted in the figure—the width of the inlet channel ($w_{in} = 30$ μm), the distance between the inlet channel and the orifice ($l_{in} = 100$ μm), the width of the orifice ($w_{or} = 30$ μm), and the length of the orifice ($l_{or} = 100$ μm). The original micrograph is shown in black; the gray lines extend the contours of the walls. (b) Bifurcation diagram showing the diameters of the bubbles as a function of the flow rate Q of the liquid ($\mu = 0.9$ mPa s) for constant pressure ($p = 76$ kPa) of gas. The first bifurcation occurs at $Q = 1.06$ μL/s. It is followed by period halving at $Q = 1.44$ μL/s. At $Q = 2.8$ μL/s, the first of a cascade of period-doubling bifurcations occurs. The cascade leads to chaos which, upon further increase of Q, gives way to a stable period-3 cycle. The solid line shows an outline of the bifurcation diagram (not to scale). The letters mark the rates of flow at which the micrographs of the period-1, period-2, period-4, and period-3 bubbling are shown in insets (c) to (f), respectively.

orifice, breaks, releases the first bubble, retracts, advances again, releases a second bubble of a different size, and the sequence repeats. As we further elevate Q, we observe a variety of nonlinear phenomena, including period doubling and halving bifurcations, and chaos. Figure 1(b) illustrates the sizes of the bubbles as a function of Q for a fixed p. As

we increased Q, monodisperse bubbling gave away to a period-2 cycle, the period then halved, and the system again produced identical bubbles. At higher values of Q, the system underwent two well demarcated period-doubling bifurcations and a transition to chaotic bubbling. Within the cascade, we observed period-2 and period-4 cycles. Period-8 orbits were unstable and hard to distinguish from the seemingly random bubbling. As we increased Q even further, chaos intermittently gave way to a stable period-3 behavior, which persisted up to the rate of flow at which the pressure applied to the gas stream was no longer sufficient to sustain the thread in the FF region.

In order to understand the dynamics of the system, we scanned the two flow parameters (p and Q) for different viscosities μ of the liquid. Figure 2(a) presents the "phase diagram" in the (p, Q) space for $\mu = 0.9$ mPa s. The diagram distinguishes regions of monodisperse bubbling from the zones in which the device produced bubbles of more than one size. We want to identify the physical quantity that controls this transition from period-1 to higher-order behavior. If the origin of the bifurcation lies in the dynamics of the gaseous thread, then frequency (f) is a plausible candidate for the control parameter. In a first-order approximation, f is proportional to the product of Q and p [Fig. 2(b)]. We also note that the viscosity of the continuous fluid does not affect the frequency appreciably [Fig. 2(c)].

The frequency of the period-1 bubbling at the point of the first bifurcation was always on the order of a few kHz: for the water-surfactant mixture, the average frequency at the first bifurcation is $f_{CR} = 5.6$ kHz (with a standard deviation of $\sigma_f = 1.3$ kHz). We therefore associate the first bifurcation with a critical frequency of bubbling. The phase diagram presented in Fig. 2(a) shows a solid line ($p \propto Q^{-1}$) that yields a critical frequency of $f_{CR} = 5$ kHz according to the phenomenological scaling detailed in Fig. 2(b). This line overlaps well with the boundary between the period-1 and period-2 responses. Experiments with more viscous ($\mu = 2.5$, 5.8, 10, 20, and 50 mPa s) solutions exhibited "phase diagrams" similar to that for $\mu = 0.9$ mPa s, and f_{CR} does not change significantly with the increase of viscosity: for the most viscous solution that we used ($\mu = 50$ mPa s), $f_{CR} = 4$ kHz, and $\sigma_f = 0.5$ kHz [Fig. 2(c)].

The origin of the bifurcations is not likely to lie in the outflow of bubbles through the orifice and outlet channel. The bubbles flow into an outlet channel that is significantly wider (500 μm) than a typical diameter of the bubble (50 to 100 μm). We assume that once the bubble has traveled a few hundred micrometers into the outlet, it can no longer affect the flow within the orifice significantly. We observed period-2 or higher-order periodic behavior, both when new bubbles broke off when preceding ones were still within (or close to) the orifice, and when they were already far downstream of the orifice. We therefore concentrate our analysis on the evolution of the tip of the gaseous thread.
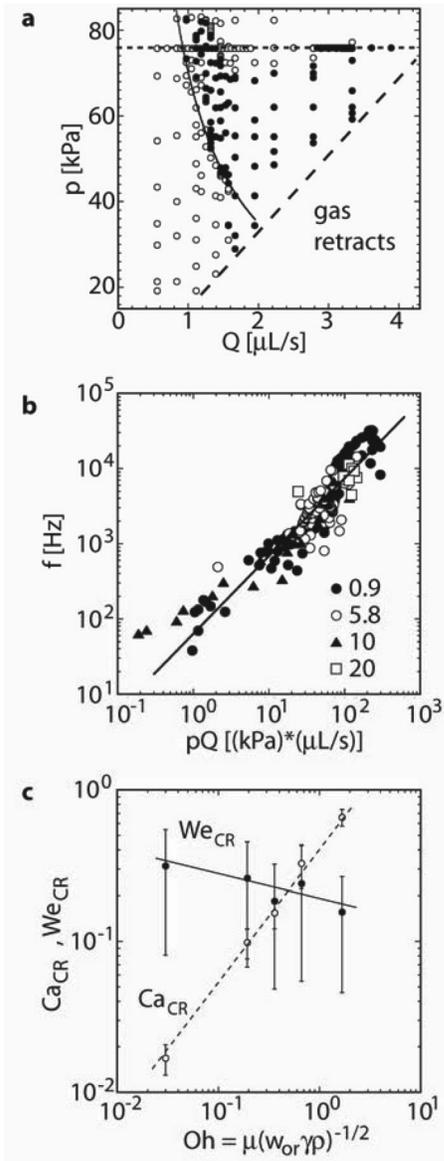
FIG. 2. (a) Phase diagram of the dynamics of the bubble generator in the p, Q space ($\mu = 0.9$ mPa s) $\bigcirc$, period-1 cycles, and $\bullet$, higher-order periodic or chaotic behavior. Below the long-dashed diagonal line, p is insufficient to force the gaseous thread through the orifice and no bubbling occurs. The horizontal, short-dashed line indicates the cut through the phase diagram (for $p = 76$ kPa) illustrated in Fig. 1(b). The solid line yields a constant frequency, $f = 5$ KHz. (b) Frequency of bubbling plotted against the product (pQ). Different symbols correspond to different viscosities μ of the liquid [values in (mPa s) given in the legend]. The solid line shows the fit $f = \alpha(Qp)^\beta$, with $\alpha = 53.3$ and $\beta = 1.04$ (regression coefficient $R = 0.94$). (c) A log-log plot of the critical capillary ($\bigcirc$) and Weber ($\bullet$) numbers as a function of the Ohnesorge number.

In order to determine the relative importance of the inertial, viscous, and capillary stresses, we calculated the capillary (Ca) and Weber (We) numbers. We distinguish between the shear and the inertial stresses *exerted on* the interface by the flowing liquid, Ca_{flow} and We_{flow}, calculated on the basis of the mean speed of the liquid through the orifice, and the shear and inertial stresses *counteracting* the capillary pressure, Ca_{inter} and We_{inter}, calculated on the basis of the frequency of bubbling and the typical length scale for the evolution of the gas-liquid interface.

The Reynolds number (Re $= \rho u L/\mu$; ρ is the density of the fluid, u its mean velocity, and L the typical length scale taken as the height of the channels $h = 25$ μm) for the externally imposed flow of liquid through the orifice ranges from Re $= 10^{-1}$ ($Q \approx 0.1$ $\mu L/s$ and $\mu = 50$ mPa s) to Re $\approx 10^2$ ($Q = 10$ $\mu L/s$ and $\mu = 0.9$ mPa s), where we used $u = Q/w_{or}h$ (where w_{or} is the width of the orifice) as the typical speed of the liquid. This range of Re indicates that both viscous and inertial effects play significant roles, but we can expect laminar flow without turbulent effects. The capillary ($Ca_{flow} = u\mu/\gamma$, where γ is the interfacial tension [39]) and Weber ($We_{flow} = \rho u^2 L/\gamma$) numbers yield the ratio of the viscous and inertial to interfacial stresses, respectively. Within the range of rates of flow and viscosities that we tested, $Ca_{flow} \in (10^{-4}, 10^{-2})$ for $\mu = 0.9$ mPa s and $Ca_{flow} \in (10^{-2}, 10^{-1})$ for $\mu = 50$ mPa s; the shear stress exerted by the liquid on the interface has little influence on its shape. In contrast, the Weber number covers a wide range of values: $We_{flow} \in (10^{-4}, 10^2)$ and suggests a crossover from regimes dominated by surface tension to those dominated by inertia.

After each breakup the thread recoils upstream of the orifice; we want to assess how much this motion is retarded by the viscous and inertial stresses. The typical speed of the interface can be estimated as $u_{inter} \approx l_{or}f$, where l_{or} is the length of the orifice, and the characteristic length scale for evolution of the tip during the recoil process is on the order of w_{or}. We use these estimates to calculate $Ca_{inter} = u_{inter}\mu/\gamma$ and $We_{inter} = \rho u_{inter}^2 w_{or}/\gamma$. We obtain $Ca_{inter} < 10^{-2}$ for $\mu = 0.9$ mPa s, $Ca_{inter} < 1$ for $\mu = 50$ mPa s, and $We_{inter} \in (10^{-4}, 10)$. These values suggest that capillary pressure dominates viscous stresses, but inertial effects can play a significant role in the relaxation of the interface after each breakup.

We now use $u_{interCR} = l_{or}f_{CR}$ to estimate the critical values of $Ca_{interCR}$ and $We_{interCR}$. For the critical capillary number, we obtain a range of values from $Ca_{interCR} \sim 10^{-2}$ (for $\mu = 0.9$ mPa s) to $Ca_{interCR} \sim 1$ ($\mu = 50$ mPa s). In contrast, $We_{interCR}$ is always on the order of 0.1; it decreases only slowly with increasing viscosity of the continuous fluid: $We_{interCR} \sim 0.3$ ($\mu = 0.9$ mPa s) to $We_{interCR} \sim 0.15$ ($\mu = 50$ mPa s) [Fig. 2(c)]. These estimates suggest that only the inertial effects can be consistently associated with the bifurcation of the bubbling process. We note here that $We_{CR} \sim 0.1$ is very similar to the values obtained for a dripping faucet [5].

The rich dynamic behavior of the FF bubble generator adds to the various nonlinear phenomena observed in the evolution of bubbles [40]. The dimensional analysis suggests that the inertial terms govern the dynamics of the tip

of the thread, and lead to the higher-order periodic and chaotic behavior. This conclusion raises the interesting question of analogy between two topologically inverted systems—a gaseous thread breaking in a flowing host fluid and a liquid dripping into an ambient atmosphere of gas. Microfluidics offer a convenient technique for probing the impact of geometrical confinement on the dynamics of breakup, and allow the experimenter to either exclude or include gravity among the forces influencing the dynamics of the system. The finding that the bifurcations are caused by inertial effects suggests that promotion of monodisperse bubbling can be achieved by a reduction of the size of the FF region (widths w_{in}, w_{or}, and lengths l_{in}, l_{or}, as defined in Fig. 1(a)]. Smaller typical length scales for the relaxation of the gaseous thread should result in larger critical frequencies of bubbling. Interestingly, the range of Reynolds and Weber numbers for which we observe this highly nonlinear dynamics is intermediate in the ranges reported for controlled formation of monodisperse bubbles in viscosity [4,41] and inertia [1,2] dominated regimes.

---

*Electronic address: pgarstecki@gmwgroup.harvard.edu
†Electronic address: gwhitesides@gmwgroup.harvard.edu

[1] A. M. Ganan-Calvo and J. M. Gordillo, Phys. Rev. Lett. **87**, 274501 (2001).
[2] A. M. Ganan-Calvo, Phys. Rev. E **69**, 027301 (2004).
[3] S. L. Anna, N. Bontoux, and H. A. Stone, Appl. Phys. Lett. **82**, 364 (2003).
[4] P. Garstecki et al., Appl. Phys. Lett. **85**, 2649 (2004).
[5] B. Ambravaneswaran, S. D. Phillips, and O. A. Basaran, Phys. Rev. Lett. **85**, 5332 (2000).
[6] F. W. Helsby and K. R. Tuson, Res. Prog. SSE **8**, 270 (1955); K. .R. Tuson, Br. J. Appl. Phys. **6**, 99 (1955).
[7] J. M. Ottino, Nature (London) **427**, 399 (2004).
[8] K. Nguyen et al., Chem. Eng. J. **64**, 191 (1996).
[9] J. Eggers, Phys. Rev. Lett. **71**, 3458 (1993).
[10] H. A. Stone, Annu. Rev. Fluid Mech. **26**, 65 (1994).
[11] I. Cohen et al., Phys. Rev. Lett. **83**, 1147 (1999).
[12] A. U. Chen, P. K. Notz, and O. A. Basaran, Phys. Rev. Lett. **88**, 174501 (2002).
[13] P. Coullet, L. Mahadevan, and C. Riera, Prog. Theor. Phys. Suppl. **139**, 507 (2000).
[14] P. Coullet, L. Mahadevan, and C. Riera, J. Fluid Mech. **526**, 1 (2005).
[15] P. Martien et al., Phys. Lett. **110A**, 399 (1985).
[16] K. Kiyono et al., Phys. Lett. A **320**, 47 (2003).
[17] A. dInnocenzo and L. Renna, Phys. Lett. A **220**, 75 (1996).
[18] P. M. C. Deoliveira and T. J. P. Penna, J. Stat. Phys. **73**, 789 (1993).
[19] D. J. Tritton and C. Egdell, Phys. Fluids A **5**, 503 (1993).
[20] A. Tufaile and J. C. Sartorelli, Phys. Lett. A **275**, 211 (2000).
[21] A. Tufaile and J. C. Sartorelli, Physica (Amsterdam) **275A**, 336 (2000).
[22] M. Y. Liu, Z. D. Hu, and J. H. Li, Chem. Eng. Commun. **191**, 1003 (2004).
[23] C. Clanet and J. C. Lasheras, J. Fluid Mech. **383**, 307 (1999).
[24] B. Ambravaneswaran et al., Phys. Rev. Lett. **93**, 034501 (2004).
[25] O. A. Basaran, AIChE J. **48**, 1842 (2002).
[26] K. R. Tuson, Br. J. Appl. Phys. **6**, 99 (1955).
[27] L. J. Mittoni, M. P. Schwarz, and R. D. Lanauze, Phys. Fluids **7**, 891 (1995).
[28] T. Thorsen et al., Phys. Rev. Lett. **86**, 4163 (2001).
[29] D. R. Link et al., Phys. Rev. Lett. **92**, 054503 (2004).
[30] T. Cubaud and C. Ho, Phys. Fluids **16**, 4575 (2004).
[31] A. Y. Fu et al., Nat. Biotechnol. **17**, 1109 (1999).
[32] J. Sinclair et al., Anal. Chem. **74**, 6133 (2002).
[33] C. L. Hansen et al., Proc. Natl. Acad. Sci. U.S.A. **99**, 16531 (2002).
[34] H. Song and R. F. Ismagilov, J. Am. Chem. Soc. **125**, 14613 (2003).
[35] S. Xu et al., Angew. Chem., Int. Ed. Engl. **44**, 724 (2005).
[36] Dow Corning table of viscosity of water/glycerol mixtures: www.dowcorning.com.
[37] The value p corresponds to the readout of the pressure reduction gauge. We neglect the pressure drop along the 30 cm tubing (ID 0.76 mm) and a 10 mm long channel (200 μm $\times$ 25 μm) connecting the gauge to the orifice region as it can be approximated to be less than 1% of the applied pressure.
[38] We measured the diameters of the bubbles on still micrographs. Standard deviations were usually smaller than the 3 μm error resulting from the limited resolution of the images.
[39] We measured the interfacial tension between nitrogen and aqueous solutions of glycerol (0 to 80% w/w) and Tween 20 surfactant [2% w/w (16 mM)] to be 35 $\pm$ 5 mN/m. In the calculations we used the value of static interfacial tension equal to 35 mN/m. The CMC of Tween 20 is 59 μM, and the aggregation number is 60. For an aqueous solution, a simple estimate yields 40 μs as the typical time it takes for a micelle to diffuse to the freshly created interface. Since the liquid flows at least at the same speed as this interface is created, we can use this time to approximate the frequency of bubbling at which diffusion will limit coverage of the interface by the surfactant. This frequency is 25 kHz, 5 times larger than the frequency at which the first bifurcation occurs. For the most viscous solution that we used (50 mPa s) the same estimate yields 0.5 kHz, so we cannot exclude dynamic surface-tension effects from playing a role in the observed phenomena.
[40] Z. C. Feng and L. G. Leal, Annu. Rev. Fluid Mech. **29**, 201 (1997).
[41] P. Garstecki, H. A. Stone, and G. M. Whitesides (to be published).